# Automated detection of long-period disturbances in seismic records; MouseTrap code

Jiří Vackář* [1], Jan Burjánek[2], and Jiří Zahradník[1]

[1] *Charles University in Prague, Faculty of Mathematics and Physics, Czech Republic*

[2] *Swiss Seismological Service, ETH Zurich, Switzerland*

November 11, 2014

## 1. Introduction

Sudden disturbances in strong-motion acceleration records, referred to as baseline offsets, are well known (Boore et al., 2002; Javelaud et al., 2011). The physical nature of this phenomenon remains unclear, although some cases are well explained by a permanent ground tilt (Graizer, 2010; Javelaud et al., 2012). The ground tilt may be caused by near-field source effects, or a local tilt at a station produced by seismic vibrations in highly heterogeneous substrata (i.e., strong gradients of material properties at small scales). Tilts are frequently observed in volcanic areas (Wielandt and Forbriger, 1999; Wiens, 2005). Delorey et al. (2008) performed an experiment showing that tilting of the instrument produces a long-period disturbance of the characteristic shape.

In these cases, the disturbances predominate on horizontal components. The disturbances can also have a purely instrumental origin (Iwan et al., 1985; Boore,

*Electronic address: vackar@geo.mff.cuni.cz

2003; Shakal and Petersen, 2001). The latter is a more suitable explanation in cases where the disturbances are also strong on the vertical component.

Similar artifacts have also been reported on different types of broad-band seismometers worldwide (Zahradník and Plešinger, 2005; Pillet and Virieux, 2007; Delorey et al., 2008). A strong disturbance is frequently characterized by a one-sided pulse in raw output velocity. A weaker disturbance is often masked by high-frequency content of the velocity record. However, it can be easily visible in the integrated output of a broad-band instrument (raw displacement) where it looks like a baseline step, whose duration equals to the seismometer corner period (Fig. 1A).

The disturbances may easily be overlooked in band-pass filtered records. Using such disturbed records can lead to wrong results in many seismic applications, e.g. the moment-tensor inversion (Zahradník and Plešinger, 2005; Zahradník et al., 2008). Similar problems might arise in the spectral estimation of the moment magnitude; the disturbed records may erroneously pass through a routine data quality control, e.g. the signal-to-noise (S/N) control (Sokos and Zahradník, 2013), because the disturbances yield apparently very large values of the S/N ratio. As seen in Fig. 1B, the disturbances cause significant spurious increase of the spectrum at low frequencies. The signal spectrum is contaminated up to frequencies much higher than the low-frequency corner of the instrument.

The main objective of this study was to develop a code for an automated detection of such disturbances aimed at removing them from the routine seismic data processing. Such a tool would also allow for systematic studies of the disturbances in order to identify and explain their origins. As an application we analyzed the disturbances in 18 years of recordings in the Swiss Digital Seismic Network.

The developed code is available as an ObsPy module (under GNU/GPL license).

## 2. Modeling the disturbances: forward problem

Many of the observed disturbances can be modeled as a seismometer response to an acceleration step on the input (Zahradník and Plešinger, 2005) (Fig. 1A). Thus, a characteristic one-sided pulse appears in the raw velocity output, which results in a baseline offset in the raw displacement (Fig. 2). Note that the step visible in the raw displacement is not a permanent displacement, but a permanent acceleration (see the acceleration scale at the right-hand side of Fig. 2D). It is because the integrated broad-band output is proportional to displacement only at frequencies above the low-frequency corner of the instrument, while it is proportional to acceleration at the low-frequency limit. Consequently, a simple integration of the instrumentally uncorrected record in its full frequency band will reveal the characteristic shape of the disturbance (smoothed ramp, see Fig. 1A).

Because of its shape, we name the disturbance an "artificial fling step" (for brevity also "fling step" in the following text). Such disturbances are well known to users of moment-tensor inversion software ISOLA (Sokos and Zahradník, 2008, 2013), because removal of disturbed records is necessary. Informally, in the community of ISOLA users, such disturbances are referred to as "mouse". We use this informal name in the developed code.

The time series $m_d(t)$ of the raw displacement disturbance caused by a unit acceleration step with zero onset time is described by

$$m_d(t) = \int_{-\infty}^{t} \int_{-\infty}^{+\infty} s(\tau)\tau h(t-\tau)\mathrm{d}\tau\mathrm{d}t \ , \qquad (1)$$

where $h(t)$ is an impulse response of the instrument to input velocity and $s(t)$ is the input unit acceleration step, i.e. the Heaviside function ($s(t) = 1$ for $t \geq 1$ and $s(t) = 0$ for $t < 0$). The inner integral is a time convolution of the input velocity ramp $s(\tau)\tau$ and instrument response $h(\tau)$. The outer integral transforms the velocity to displacement.

The disturbances often occur simultaneously on three component recordings; in another words, the causative acceleration step has three components as well. Thus we use 4 parameters for the description of a real fling step: time $t_0$ of

the onset of the input acceleration step, amplitude $A$ of the acceleration step and two spatial angles—horizontal azimuth $\phi$ and its inclination $\theta$ from the horizontal plane. The east, north and vertical components of the raw displacement disturbance recording are therefore

$$m_E(t) = m_d(t - t_0)A \sin\phi \cos\theta \tag{2}$$

$$m_N(t) = m_d(t - t_0)A \cos\phi \cos\theta \tag{3}$$

$$m_Z(t) = m_d(t - t_0)A \sin\theta \tag{4}$$

# 3. Fitting the disturbances: inverse problem

Explaining a recorded disturbance by the synthetic fling step formally means solving an inverse problem with 4 parameters: $t_0$, $A$, $\phi$, and $\theta$. In order to have a unique solution, $A$ must be positive and the angles $\phi$ and $\theta$ are in intervals 0–360° and −90 to +90°, respectively. The inverse problem is solved by the least-squares method (LSQ) to minimize the $L^2$-norm difference between the observed record and synthetic fling step. The agreement is quantified by variance reduction ($VR$). Analytical expressions of the partial derivatives with respect to $A$, $\phi$, and $\theta$ are used in the LSQ fitting (see Appendix A for details). The values of $t_0$ are selected from a grid of values and the inverse problem is solved for the other three parameters in each grid point; then the corresponding parameters for $t_0$ with the highest $VR$ are selected.

Besides VR we also need to define a criterion—whether the fling step is present or absent. To this goal we evaluate an existence criterion

$$mp = VR - \frac{|t_0 - t_S|}{const}\ , \tag{5}$$

where $t_S$ is the $S$-wave arrival. The term $|t_0 - t_S|/const$ serves to penalize step-like disturbances not related to the earthquake in order to exclude false detection due to noise. The penalty term was motivated by the observation that most fling steps occur shortly after the $S$-wave arrival ($t_0 \geq t_S$). The term $const$ is a numerical constant chosen to be much larger than $t_0 - t_S$ in case of earthquake-induced fling step ($const = 50\,\mathrm{s}$ in application of this paper, chosen ad hoc after

few preliminary tests). If the *const* is too low, the earthquake-induced fling steps might be excluded; if it is too high, many cases where the long-period noise is fitted by synthetic fling step, such as in Fig. 3D, are taken into account. After visually inspecting dozens of disturbances with various $mp$ values, we set up an empirical criterion that the cases with $mp > 0.7$ are fling steps, $mp < 0.2$ are not fling steps, and cases $0.2 < mp < 0.7$ require visual inspection to distinguish whether the fling step is present or not. There are examples of records and fitted synthetic disturbances in Fig. 3: Record of station SIMPL (Fig. 3A, $mp = 0.75$) is a typical example of a strong disturbance. Record of MRGE (Fig. 3B, $mp = 0.63$) is unclear: when we look at record in detail, the baseline trend starts seconds before the earthquake and its shape differs from the synthetic disturbance. At station BERNI (Fig. 3C, $mp = 0.28$) the disturbance might be present, although it is weak and the shape is not fitted perfectly. In record of ZUR (Fig. 3D, $mp = 0.12$) there is a relatively well fitted long-period noise, but with relation neither to an earthquake nor to the studied disturbance.

# 4. MouseTrap code

We implemented the described approach into an ObsPy module called `MouseTrap`. The module consists of the following functions:

**mouse.create** Calculates the instrument output for a given transfer function and a unit acceleration step on the input.

**PrepareRecord** Removes the before-event mean value, integrates record into displacement, and analyzes the signal-to-noise ratio of the record (ratio of before-event maximum to record maximum). Testing signal-to-noise ratio is necessary to prevent explaining strong long-period noise as a disturbance.

**mouse.fit_3D** Fits a given three-component record with a synthetic fling step.

**mouse.exist** Distinguishes whether the fling step is present according the fit value, synthetic fling step amplitude and its ratio to record amplitude. The

output can be optionally the binary value (0, 1), or the $mp$ value.

**mouse.params** Returns the parameters $t_0$, $A$, $\phi$, and $\theta$ of the detected fling step.

**mouse.plot** Plots the comparison between observed record and synthetic fling step.

The module is published under GNU/GPL license, and available at `http://geo.mff.cuni.cz/~vackar/mouse`. The detailed documentation and a few examples are also on the website. Running the code requires Python interpreter (version 2.7.x) with ObsPy (Beyreuther et al., 2010) and Matplotlib (Hunter, 2007) libraries installed. The module can be used for two tasks—the fling step detection in a single record, or the detection of fling steps in a set of records of a seismic network. The latter requires earthquake catalog in machine-readable or database form.

# 5. Automated detection of disturbances in a seismic network

Here we demonstrate the code capabilities through a systematic detection of fling steps using a database of seismic records. The source code of this procedure (`SwissMouse`) can be found at the website mentioned above and the results of its application to Swiss Digital Seismic Network are described in the following section. The algorithm flowchart is shown in Fig. 4.

The procedure starts with event selection from the database. For each earthquake, a set of stations is selected in the distance range according to magnitude and the Swiss ground motion prediction equation (GMPE) (Edwards and Fäh, 2013; Cauzi et al., 2014). We take into account the stations where the exceedance of a fixed acceleration value is expected. As a posteriori verification we checked that only few detected disturbances lie next to the cut-off line of the criterion. Waveform data and poles and zeros (PAZ) are downloaded from the ArcLink

server. The signal-to-noise ratio (ratio of before-event maximum to record maximum) is tested, and the unfavorable records are skipped. Simple parameters of the records, such as epicentral distance and azimuth, as well as the PGA, PGV, and PGD values are evaluated. In addition to standard PGA and PGV values, these values were also calculated in different frequency bands, i.e. the record was band-pass filtered and then maximal values determined. Next, the fling step modeling is applied using the `MouseTrap` code and the inverted parameters of the fling step are stored in an SQL database. The entire process is fully automated, but the comparison between observed and synthetic waveform is also plotted for possible visual inspection. Last but not least, correlation plots and histograms, which are discussed in the following chapter, are automatically plotted using pre-defined SQL queries.

# 6. Case study: disturbance detection in 18 years of record of Swiss Digital Seismic Network

We examined 18 years of records of Swiss Digital Seismic Network using the developed `MouseTrap` and `SwissMouse` codes. The purpose was to test the detection algorithm and obtain a set of fling steps for a rough evaluation of their properties.

The magnitude-distance criterion was met by 6,240 broad-band records, but only 1,126 records were passed to further analysis (see Tab. 1 for details). From the analyzed records, in 83 cases a fling step was detected with no doubt ($mp > 0.7$). Most of the detected disturbances are in records where the seismic signal is significantly below the saturation level. Another 129 cases were unclear ($0.7 > mp > 0.2$), and a visual inspection was necessary for decision about the fling step existence.

The main properties of fling steps in our dataset can be briefly summarized as follows: Some directions of the fling step are more frequent. Namely, many of fling steps were observed in azimuth $\phi$ equal to 30°, 270°, and 150°, or the opposite directions (Fig. 5A). These azimuths coincide with directions of the three inclined

pendulums in Galperin's design seismographs (like Streinecken STS-2 and Nanometrics Trillium T40, which are the most frequent broad-band instruments in the Swiss Digital Seismic Network). Most of the disturbances are horizontal ($\theta = 0$), but a significant number have the inclination $\theta$ close to $\pm 35^\circ$ (Fig. 5B). The inclination of the pendulums in the Galperin's seismographs is 35.3°. Therefore, these observations might indicate the instrumental origin of the disturbances. Looking at individual stations, there are stations where most of the fling steps are horizontal, but correlated neither with the azimuth of the pendulum, nor with the back-azimuth of the event, and there are some other stations where most of the fling steps are in the azimuth and inclination of one preferred pendulum (Fig. 5C and Fig. 5D).

Fling steps are more common near the epicenter and at higher magnitudes (Fig. 6A). This is probably related to stronger ground shaking, but does not correlate well with PGA, PGV, or PGD. Beside these parameters the ratio fling-step / no-fling-step is also dependent on epicentral distance (Fig. 6B).

We also evaluated the fling-step / no-fling-step ratio at different seismograph types (Fig. 7A). The ratio is similar for all three types of the broad-band instruments used in Swiss Digital Seismic Network. There are minor differences between broad-band instruments, but this result is partly influenced by the presence or absence of events near to the investigated stations.

When we looked at fling step count at the individual investigated stations (Fig. 7B), a large variability was found, ranging from stations very rich in fling steps to stations with no fling step at all. Some of the stations where fling steps are common are situated very close to some earthquakes, so fling steps are mostly caused by near events (e.g. stations VANNI, FUORN). But there are also stations (e.g. SIMPL, AIGLE), where the fling step occurrence is high independently of the epicentral distance of the event (Fig. 7C and Fig. 7D).

Finally, the disturbance occurrences in Swiss network have no simple rules and can be hardly predicted. There are stations, where the disturbance occurrence is much more probable; which might indicate some instrumental problem. Never-

theless we demonstrated their systematic existence especially at stations within short epicentral distances. Such stations are crucial in moment tensor inversions of weak events. The tool developed here is capable to detect and characterize such disturbances, so the disturbed records could be easily removed from processing without considering their origin.

# 7. Conclusion and discussion

We developed a code `MouseTrap` for automated detection of fling step disturbances in seismic records. The program is available under free license at website `http://geo.mff.cuni.cz/~vackar/mouse`. The spurious input acceleration step and the instrument response explain many of the observed disturbances very well. Fitting the synthetic disturbance into real records provides four parameters of the input acceleration step, namely its onset time $t_0$, amplitude $A$, azimuth $\phi$, and inclination $\theta$. The code can be applied either to an individual record or to a set of records with metadata in a database.

We expect the code to be useful in many applications for automatic data processing, e.g. waveform inversion and S/N ratio evaluation, where detection and removal of contaminated records is a must.

We also developed the code `SwissMouse` for automated analysis of fling step existence in broad-band records of Swiss Digital Seismic Network over the last 18 years, at stations close to located events. Fling steps are present at all types of studied broad-band instruments, at many different stations. We observed a higher percentage of fling steps at some stations. Azimuths of fling steps remain the same at some (but not all) stations. In particular there is a higher occurrence of fling steps with azimuths 30°, 90°, and 150°. Most of the fling steps are horizontal, but a significant number have inclination $\sim 35°$. These preferred directions are very likely related to pendulums in Galperin's design seismometers, so these cases are probably of instrumental origin. There is a good reason (supported by limited authors' experience) to expect, that in instruments operating with pendulums in N, E, Z setup, such as e.g. Guralp CMG 3-T, the disturbances might sometimes be

preferentially related to a single component. The fling steps are more common at records with higher PGA and PGV, near the source, and at higher magnitudes (M 1–4 mostly examined). Besides this paper we have also observed such disturbances at short-period instruments, where they are naturally characterized by much shorter durations than at broad-band seismometers.

There are also similar disturbances which can be described as instrument response to a spurious step in the input velocity (Zahradník and Plešinger, 2010), which can be explained as caused by saturation in the force-balance system. These might be implemented in future updates of the `MouseTrap` code, including diagnostics of a joint occurrence of both kinds of disturbances. Another challenging issue is to develop the fling step detection in continuous records.

# 8. Acknowledgement

We are grateful to Philipp Kästli for his help with using SeisComP database. We would like also to thank Yannik Behr and Carlo Cauzzi for useful advice and Benjamin Edwards for language correction. The work was supported by the Czech Republic grants SVV 2014-260096, GAČR 14-04372S, and GAUK 496213. The used dataset comes from Swiss Seismic Network operated by Swiss Seismological Service, with data from neighboring countries operated by INGV, ZAMG, and University of Genoa included.

# References

Beyreuther, M., R. Barsch, L. Krischer, T. Megies, Y. Behr, and J. Wassermann (2010). ObsPy: A Python Toolbox for Seismology, *Seismol. Res. Lett.*, **81**, 530–533.

Boore, D. M., Ch. D. Stephens, and W. B. Joyner (2002). Comments on baseline correction of digital strong-motion data: examples from the 1999 Hector Mine, California, earthquake, *Bull. Seismol. Soc. Am.,* **92**, 1543–1560.

Boore, D. M. (2003). Analog-to-digital conversion as a source of drifts in displacements derived from digital recordings of ground acceleration, *Bull. Seismol. Soc. Am.,* **93**, 2017–2024.

Cauzzi, C., B. Edwards, D. Fäh, J. Clinton, S. Wiemer, P. Kästli, G. Cua, and D. Giardini (2014). New predictive equations and site amplification estimates for the next-generation swiss shakemaps, *submitted to Geophys. J. Int.*

Delorey, A. A., J. Vidale, J. Steim, and P. Bodin (2008). Broadband sensor nonlinearity during moderate shaking. *Bull. Seismol. Soc. Am.,* **98**, 1595–1601.

Edwards, B. and D. Fäh (2013). A stochastic ground-motion model for Switzerland, *Bull. Seismol. Soc. Am.,* **103**, 78–98.

Graizer, V. (2010). Strong motion recordings and residual displacements: What are we actually recording in strong motion seismology?, *Seismol. Res. Lett.*, **81**, 635–639.

Hunter, J. D. (2007). Matplotlib: A 2D graphics environment, *Computing in Science and Engineering*, **9**, 90–95.

Iwan, W. D., M. A. Moser, and C. Y. Peng (1985). Some observations on strong-motion earthquake measurement using a digital accelerograph, *Bull. Seismol. Soc. Am.,* **75**, 1225–1246.

Javelaud, E. H., T. Ohmachi, and S. Inoue (2011). A quantitative approach for estimating coseismic displacements in the near field from strong-motion accelerographs, *Bull. Seismol. Soc. Am.,* **101**, 1182–1198.

Javelaud, E. H., T. Ohmachi, and S. Inoue (2012). Estimating small permanent rotation from strong-motion records: What is comparison with external measurements telling us?, *Bull. Seismol. Soc. Am.,* **102**, 2257–2263.

Pillet, R., and J. Virieux (2007). The effects of seismic rotations on inertial sensors, *Geophys. J. Int.,* **171**, 1314–1323.

Shakal, A. F., and C. D. Petersen (2001). Acceleration offsets in some FBA's during earthquake shaking (abstract), *Seismol. Res. Lett.*, **72**, 233.

Sokos, E. N., and J. Zahradník (2008). ISOLA a Fortran code and a Matlab GUI to perform multiple-point source inversion of seismic data, *Computers and Geosciences*, **34**, 967–977.

Sokos, E. N., and J. Zahradník (2013). Evaluating centroid-moment-tensor uncertainty in the new version of ISOLA software, *Seismol. Res. Lett.*, **84**, 656–665.

Wielandt, E., and T. Forbriger, (1999). Near-field seismic displacement and tilt associated with the explosive activity of Stromboli, *Ann. di Geofis.*, **42**, 407–416.

Wiens, D. A., S. H. Pozgay, P. J. Shore, A. W. Sauter, and R. A. White (2005). Tilt recorded by a portable broadband seismograph: The 2003 eruption of Anatahan Volcano, Mariana Islands, *Geophys. Res. Lett.*, **32**, L18305.

Zahradník, J., J. Janský, and V. Plicka (2008). Detailed waveform inversion for moment tensors of M∼4 events; examples from the Corinth Gulf, Greece, *Bull. Seismol. Soc. Am.,* **98**, 2756–2771.

Zahradník, J., and A. Plešinger (2005). Long-period pulses in broadband records of near earthquakes, *Bull. Seismol. Soc. Am.,* **95**, 1928–1939.

Zahradník, J., and A. Plešinger (2010). Toward understanding subtle instrumentation effects associated with weak seismic events in the near field, *Bull. Seismol. Soc. Am.,* **100**, 59–73.

| | |
|---|---|
| **Records total** | **6,240** |
| Skipped records | 5,114 |
| problems with download | 1,087 |
| unfavorable signal-to-noise ratio | 3,965 |
| gap in data | 42 |
| no PAZ file | 20 |
| **Analyzed records** | **1,126** |
| no fling step detected | 914 |
| fling step is unclear (visual inspection necessary) | 129 |
| **fling step detected with no doubt** | **83** |

Table 1: Statistics of the analyzed records. The records were analyzed by code `SwissMouse` while it was applied on 18-years set of Swiss data.

(A)

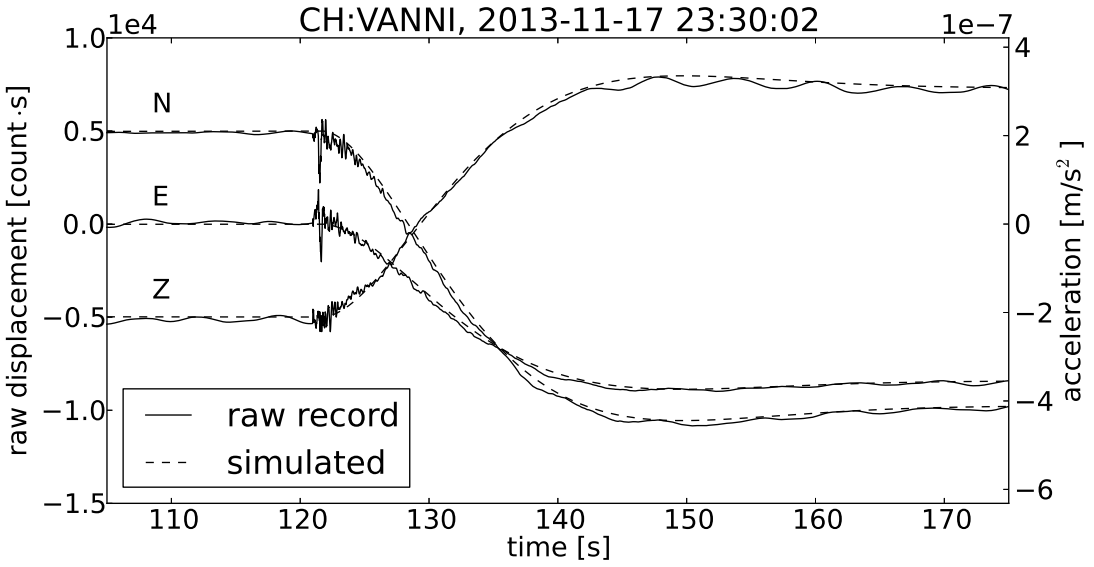


(B)

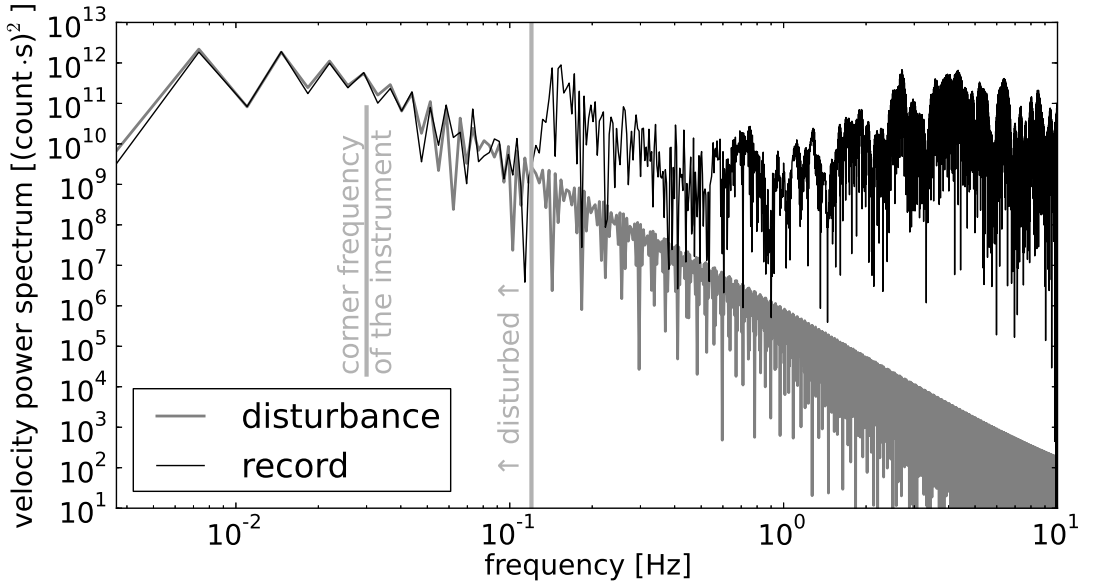


Figure 1: **A)** Example of a step-like disturbance in the integrated output (raw displacement) of the Nanometrics Trillium T40 seismometer. The disturbance is well fitted by the simulated instrument response to an acceleration step of amplitude $A = 8.7 \cdot 10^{-7}\,\mathrm{m \cdot s^{-2}}$, azimuth $\phi = 209.7°$, and inclination $\theta = 35.9°$. The recorded earthquake has magnitude $M_{Lh} = 1.7$ (Swiss Seismological Service), its epicentral distance is 1.9 km. **B)** Power spectrum of raw velocity ($Z$ component) and of the disturbance. The disturbance dominates in the spectrum up to frequency ∼0.12 Hz.

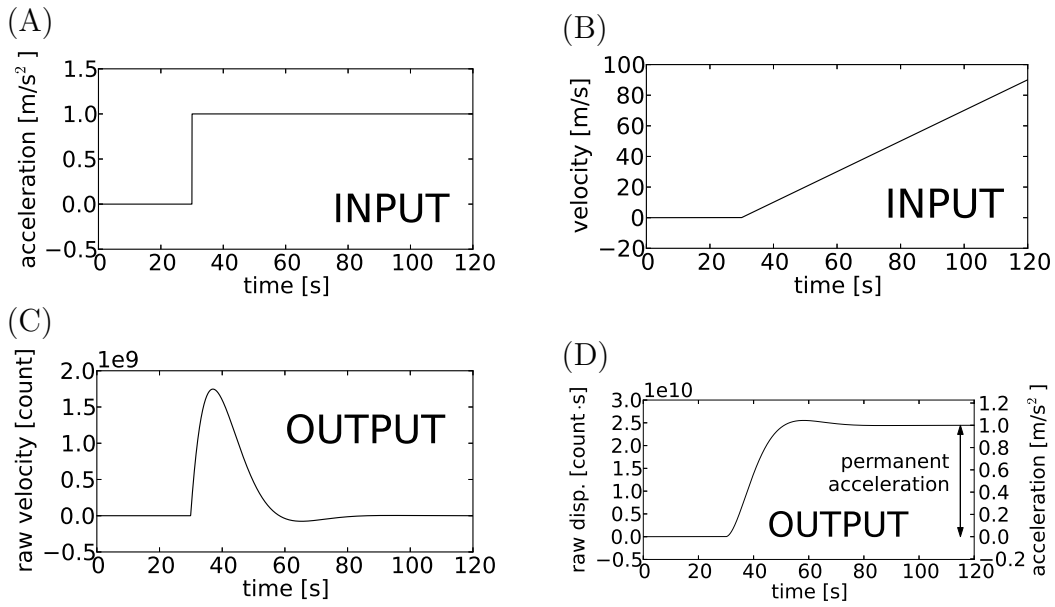


Figure 2: Modeling a disturbance. The input acceleration step (A) is equivalent to the velocity ramp (B). After applying the instrumental response (here for Nanometrics Trillium T40) we get a characteristic one-sided pulse in the output raw velocity (C), and a step-like disturbance in the raw displacement (D). The right-hand scale of panel D corresponds to the low-frequency limit of integrated broad-band output which is proportional to acceleration.

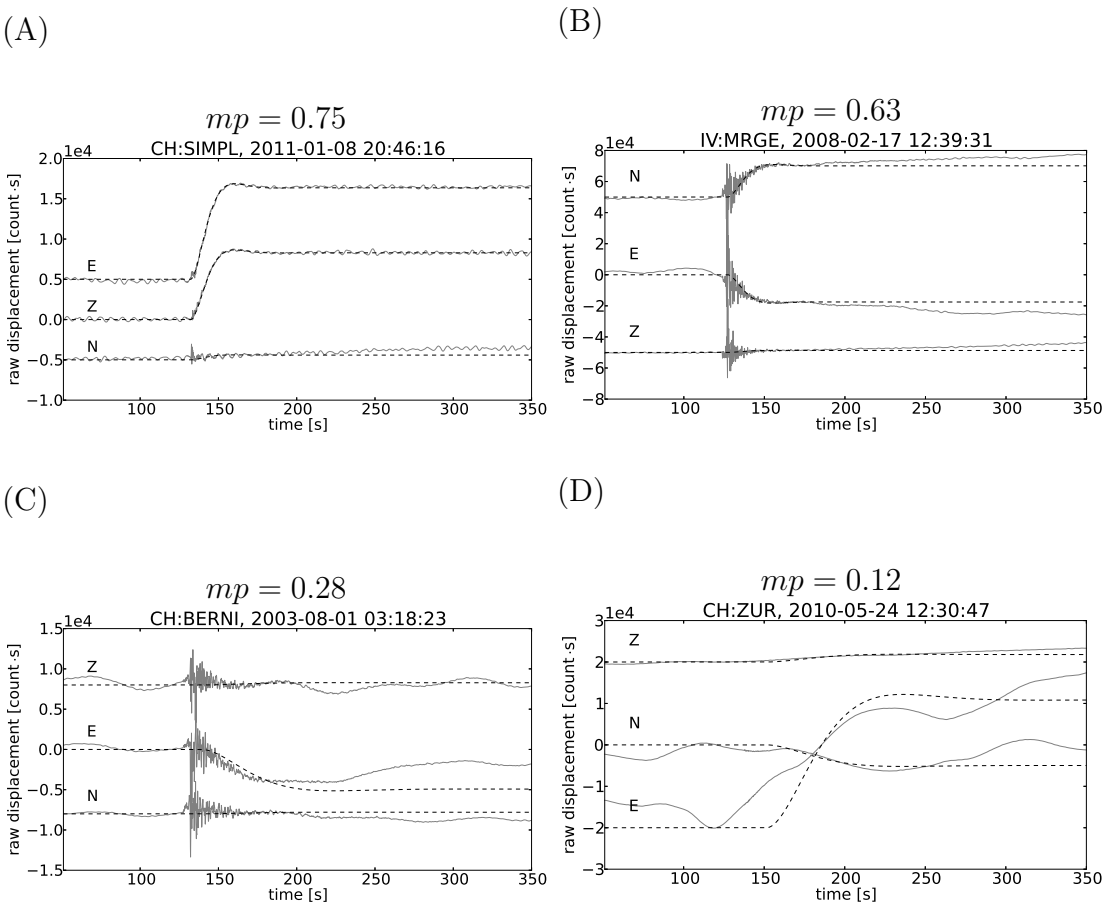


Figure 3: Agreement between observed records (solid line) and fitted synthetic disturbances (dashed line) for different values of the existence criterion $mp$.

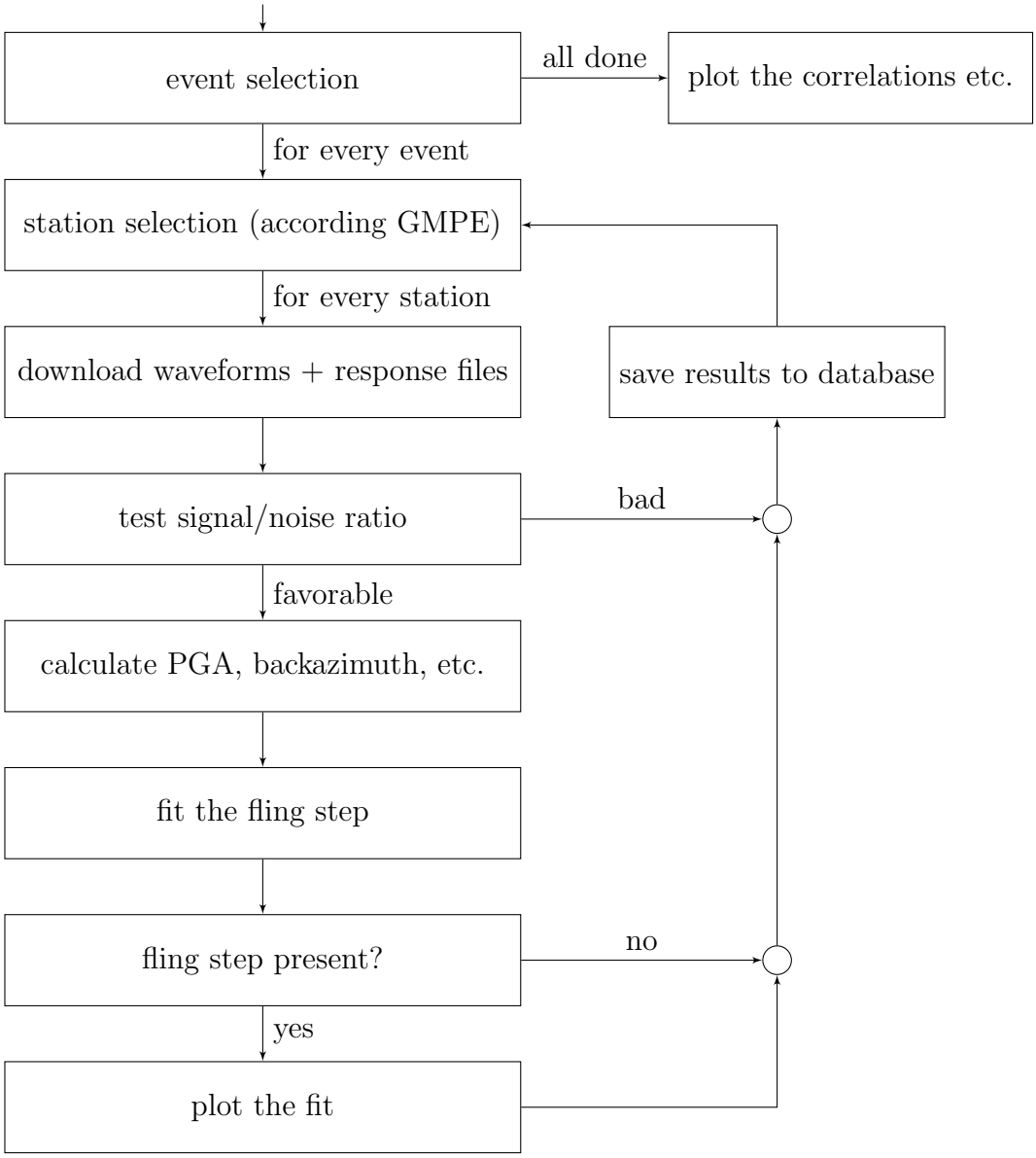


Figure 4: Flowchart of the systematic detection of fling steps with database of records using `SwissMouse` code.

(A)

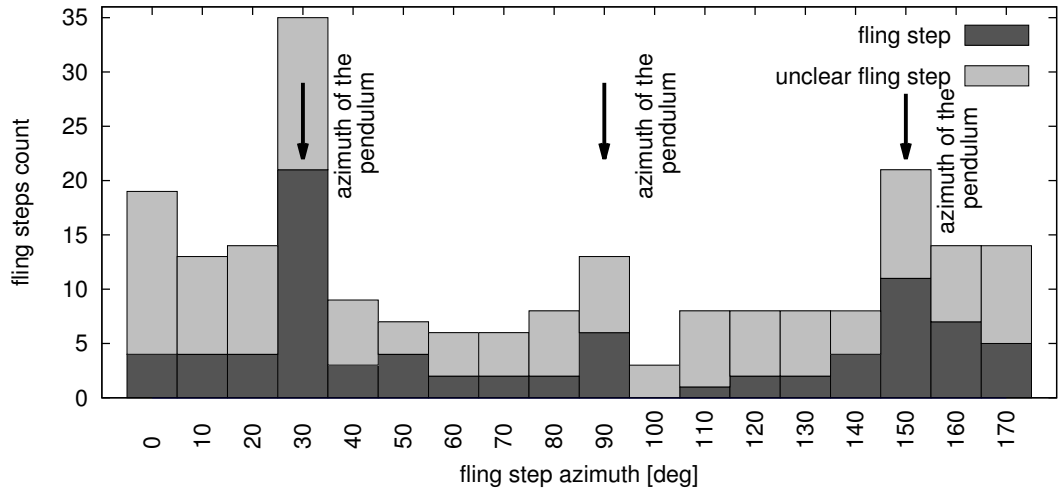


(B)

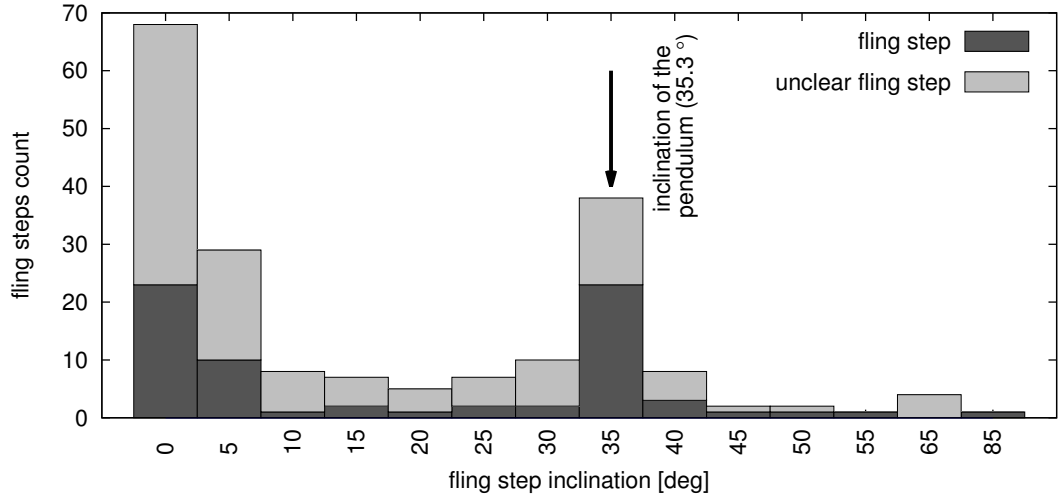


(C)

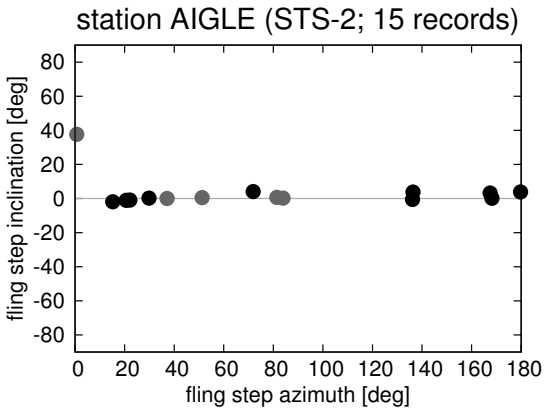


(D)

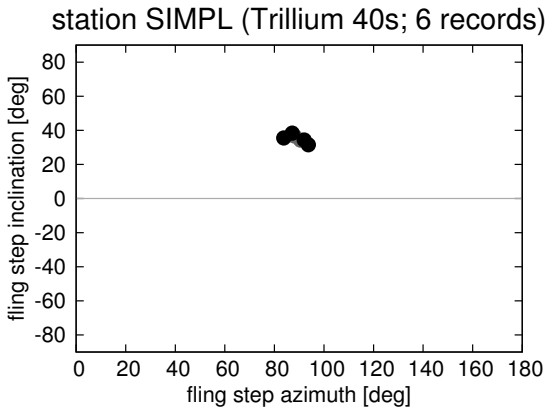


Figure 5: Azimuths (A) and inclination (B) of the step-like disturbances in the 18-years dataset of disturbances detected in the Swiss Seismic Network. For better visibility, the azimuth is restricted to the interval 0–180° and inclination to 0–90° because some of disturbances are in direction of the pendulum and some in the opposite direction. There are some stations where the fling steps are nearly horizontal and in different azimuths (C), and some other stations where all the

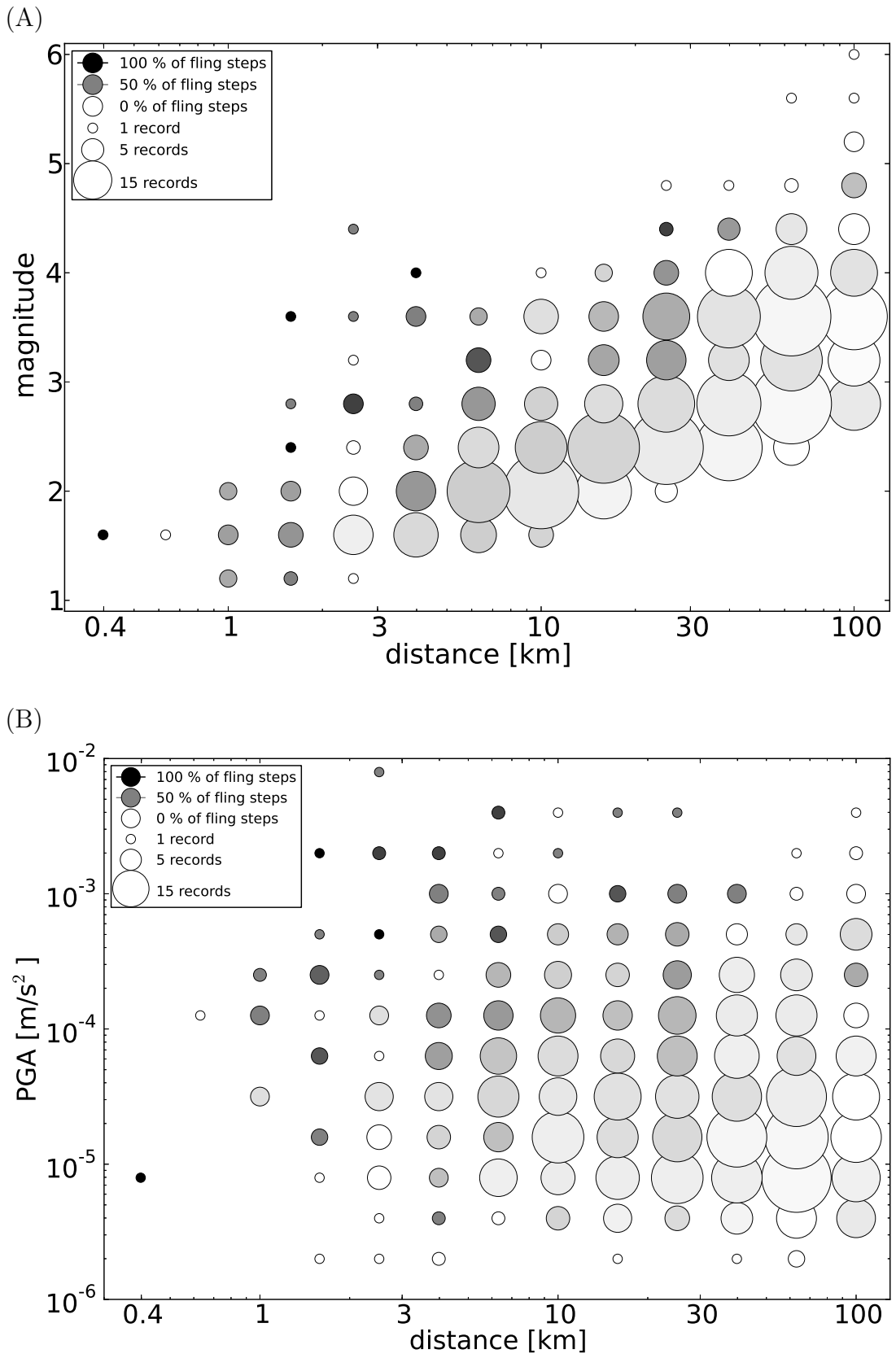


Figure 6: Fling steps are more common near the epicenter and at higher magnitudes (A). Fling steps are more common at higher PGA (B). The magnitude (A) comes from Swiss Seismological Service earthquake catalogue, moment magnitude $M_w$ and local magnitudes $M_L$ and $M_{Lh}$ are used for different events.

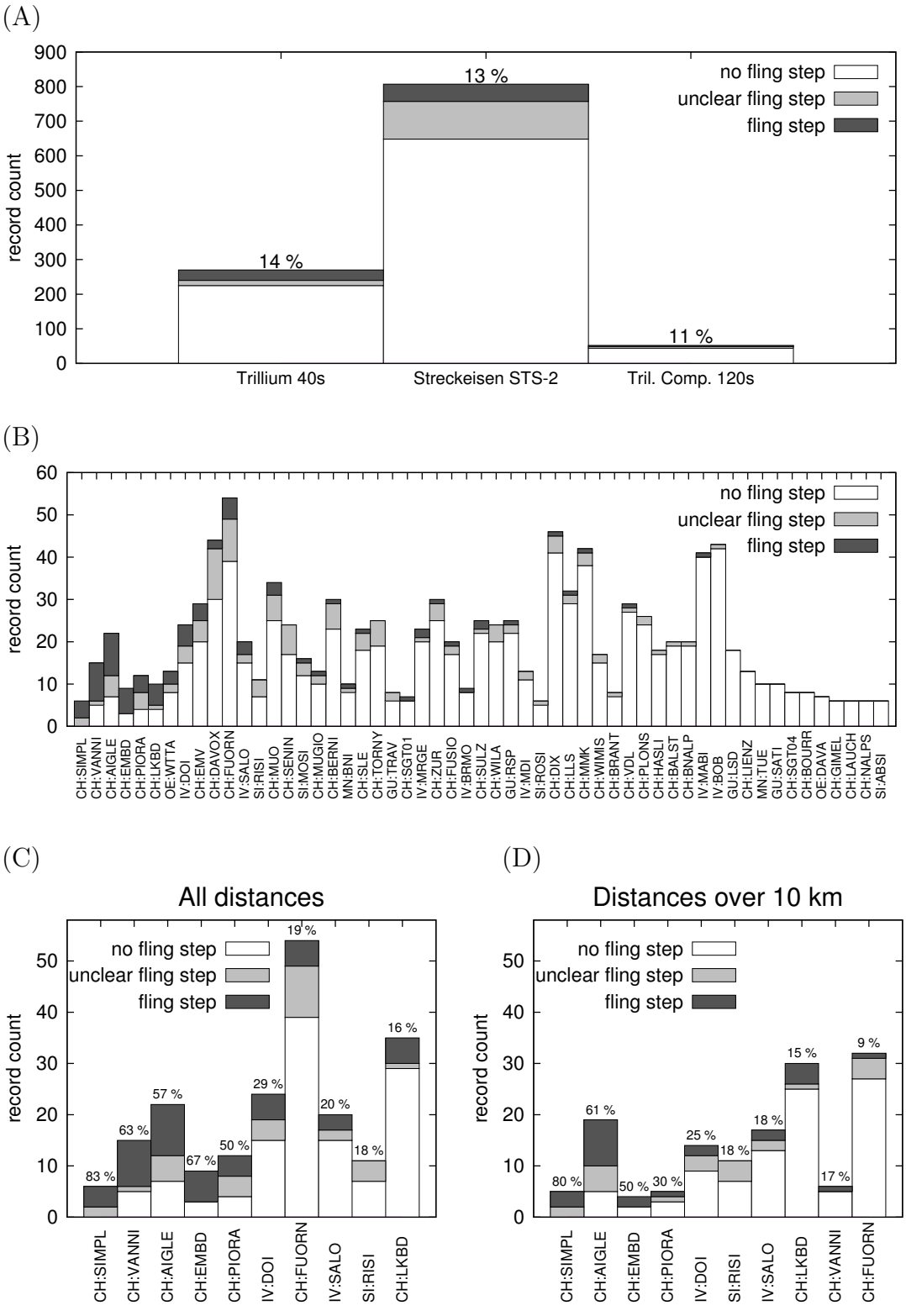


Figure 7: Fling steps count at studied broad-band sensors (A). Fling steps counts at the studied stations with more than 5 records (B). Fling step count at selected stations for events in all epicentral distances and for epicentral distances over 10 km (C and D).

# Appendix A

Analytical expressions of partial derivatives are used during least-squares fitting of observed record by synthetic fling step.

Let us have a three component record with north-south, east-west, and vertical components $s_i^N$, $s_i^E$, and $s_i^Z$, respectively, where $i$ indexes time samples. We want to minimize the difference between the record and a synthetic disturbance $m_i$ by finding proper amplitude $A$, azimuth $\phi$, and inclination $\theta$ of the disturbance. The difference in the $L^2$-norm

$$\sum_i \left(s_i^N - Am_i \cos\phi\cos\theta\right)^2 + \sum_i \left(s_i^E - Am_i \sin\phi\cos\theta\right)^2 + \sum_i \left(s_i^Z - Am_i \sin\theta\right)^2 \tag{6}$$

should be minimal, so its partial derivatives should be zero.

From $\frac{\partial}{\partial\phi} = 0$ we get

$$\frac{\sum_i m_i s_i^E}{\sum_i m_i s_i^N} = \frac{\sin\phi}{\cos\phi} = \tan\phi\ . \tag{7}$$

From $\frac{\partial}{\partial\theta} = 0$ we get

$$\frac{\sum_i m_i s_i^Z}{\sum_i m_i \left(s_i^N\cos\phi + s_i^E\cos\phi\right)} = \frac{\sin\theta}{\cos\theta} = \tan\theta\ . \tag{8}$$

From $\frac{\partial}{\partial A} = 0$ we get

$$\frac{\sum_i m_i \left(s_i^N\cos\phi\cos\theta + s_i^E\sin\phi\cos\theta + s_i^Z\sin\theta\right)}{\sum_i m_i^2} = A\ . \tag{9}$$